Journal of the Physical Society of Japan **85**, 064705 (2016)
http://doi.org/10.7566/JPSJ.85.064705

Superconductivity in a Misfit Phase That Combines the Topological Crystalline Insulator $Pb_{1-x}Sn_xSe$ with the CDW-Bearing Transition Metal Dichalcogenide $TiSe_2$

Huixia Luo[1]*, Kai Yan[2], Ivo's Pletikosic[3,4], Weiwei Xie[1], Brendan F. Phelan[1], Tonica Valla[3], and Robert J. Cava[1†]

[1]*Department of Chemistry, Princeton University, Princeton, NJ 08544, U.S.A.*
[2]*School of Engineering, Brown University, Providence, RI 02912, U.S.A.*
[3]*Condensed Matter Physics and Materials Science Department, Brookhaven National Lab, Upton, NY 11973, U.S.A.*
[4]*Department of Physics, Princeton University, Princeton, NJ 08544, U.S.A.*

(Received March 19, 2016; accepted April 15, 2016; published online May 13, 2016)

We report the characterization of the misfit compound $(Pb_{1-x}Sn_xSe_2)_{1.16}(TiSe_2)_2$ for $0 \le x \le 0.6$, in which a [100] rocksalt-structure bilayer of $Pb_{1-x}Sn_xSe$, which is a topological crystalline insulator in bulk form, alternates with a double layer of the normally non-superconducting transition metal dichalcogenide $TiSe_2$. The x dependence of T_c displays a weak dome-like shape with a maximum T_c of 4.5 K at $x = 0.2$; there is only a subtle change in T_c at the composition where the trivial to topological transition occurs in bulk $Pb_{1-x}Sn_xSe$. We present the characterization of the superconductor at $x = 0.4$, for which the bulk $Pb_{1-x}Sn_xSe$ phase is in the topological crystalline insulator regime. For this material, the Sommerfeld parameter $\gamma = 11.06\,\mathrm{mJ\,mol^{-1}\,K^{-2}}$, the Debye temperature $\Theta_D = 161$ K, the normalized specific heat jump value $\Delta C/\gamma T_c = 1.38$ and the electron–phonon constant value $\lambda_{ep} = 0.72$, suggesting that $(Pb_{0.6}Sn_{0.4}Se)_{1.16}(TiSe_2)_2$ is a BCS-type weak coupling superconductor. This material may be of interest for probing the interaction of superconductivity with the surface states of a topological crystalline insulator.

1. Introduction

A broad family of layered ternary chalcogenides, the so-called misfit compounds, has recently been reported. They are generally described as $[(MX)_{1+x}]_m(TX_2)_n$, where M = Sn, Pb, Sb, Bi, or Ln (lanthanide); T = Ti, V, Cr, Nb, Mo, Ta, or W; X = S, Se, or Te; $0.08 < x < 0.28$; and m and n are integers indicative of the number of MX rocksalt double layers stacked in an alternating fashion with TX_2 dichalcogenide layers (n and $m = 1, 2, 3, 4$).[1–8] The MX and TX_2 layers have different symmetry and periodicity, matching in size in one crystallographic in-plane direction but not matching (i.e., misfitting) in the second in-plane direction, yielding the oddly non-stoichiometric formulas. The misfit is accommodated at the interface between close packed chalcogen layers in the TX_2 part and the polarizable MX layers. The individual rocksalt and dichalcogenide layers in the misfit compounds are somewhat distorted from those of the constituent simple MX and TX_2 materials,[8] meaning that the electronic structures of the constituent layers are likely similar but not identical to those of the individual bulk MX and TX_2 compounds. Our angle resolved photoemission spectroscopy (ARPES) data, described below, shows for example that charge is transferred from the MX layers to the TX_2 layers in the current case.

The wide variations in M, T, X, m, and n allowed in the family lead to many different physical properties.[5,9–16] The current case involves a misfit phase based on the stacking of [100] PbSe double layers and [001] $TiSe_2$ layers. PbSe is a trivial semiconductor (i.e., the sequence of the electronic bands near the Fermi energy is as expected in a simple electronic picture) and has a direct band gap of 0.27 eV at room temperature.[17,18] Recently it has been shown, however, that the bulk $Pb_{1-x}Sn_xSe$ rocksalt compound undergoes an inversion of the electronic band energy sequence at $x = 0.23$ and becomes a topological crystalline insulator, with, correspondingly, protected topological surface states.[18] When PbSe is stacked in a misfit compound with $NbSe_2$, the intrinsic T_c of $NbSe_2$ (7 K) is degraded and superconductivity results for $(PbSe)_{1.14}(NbSe_2)_n$ for $n = 2$ and 3 at 3.4 and 4.8 K respectively, with no reported superconductivity for $n = 1$ down to 2 K.[19] When stacked with non-superconducting 1T-$TiSe_2$,[20–23] on the other hand, the resulting misfit compound $(PbSe)_{1.16}(TiSe_2)_2$ is reported to be a superconductor with $T_c = 2.3$ K.[24] Motivated by these observations, here we report the superconductivity that results when Sn partially substitutes for Pb in the $(Pb_{1-x}Sn_xSe)_{1.16}(TiSe_2)_2$ misfit compound solid solution, in order to determine whether the superconductivity is still present at the composition in the MX layers where bulk $Pb_{1-x}Sn_xSe$ is a topological crystalline insulator. It is superconductor, and we observe only a subtle change in T_c vs x at the composition where the trivial to topological crossover is found in $Pb_{1-x}Sn_xSe$.

2. Experimental

$(Pb_{1-x}Sn_xSe_2)_{1.16}(TiSe_2)_2$ single crystals and polycrystals were grown in three steps. First, mixtures of high-purity fine powders of Pb (99.9%), Sn (99.5%), Ti (99.9%), and Se (99.999%) in the appropriate stoichiometric ratios were mixed and heated in sealed evacuated silica tubes at a rate of 1 °C/min to 700 °C and held there for 48 h. Subsequently, the as-prepared powders were reground and heated at a rate of 3 °C/min to 900 °C and held there for 16 h. Finally, larger and smaller crystals from the as-prepared powders were grown in the third step by the chemical vapor transport (CVT) method, using $SeCl_4$ as a transport agent. 50 mg of the as-prepared powders of $(Pb_{1-x}Sn_xSe_2)_{1.16}(TiSe_2)_2$ were mixed with 35 mg $SeCl_4$, sealed in evacuated silica tubes and heated for one week in a two-zone furnace, where the temperature of source and growth zones were fixed at 750 and 680 °C, respectively. After one week, polycrystalline samples and some shiny, plate-like grey single crystals of $(Pb_{1-x}Sn_xSe_2)_{1.16}(TiSe_2)_2$ were found at the cold end. Property meas-

urements were performed on the crystals and polycrystals (collections of small single crystals) from the cold end. This synthetic method differs from the one reported previously[24] but is suitable for uniformly preparing the samples in the solid solution series studied here.

The identity and phase purity of the materials studied were determined by powder X-ray diffraction (PXRD) on polycrystals and crystal plates using a Bruker D8 ECO diffractometer with Cu Kα radiation and a Lynxeye detector. To determine the phase purity, LeBail fits were performed on the powder diffraction data through the use of the FULLPROF diffraction suite using Thompson–Cox–Hastings pseudo-Voigt peak shapes.[25] Single crystals selected from partially crushed crystalline samples were studied on a Bruker D8 ECO single crystal diffractometer with Cu Kα radiation to fully verify that the materials matched the misfit structure previously reported for the Pb-containing end member. The compositions of the materials were determined by employing Energy dispersive X-ray fluorescence spectroscopy (EDX) on the crystals using a Quanta 200 FEG ESEM electron microscope operated at 20 kV; PbSe, SnSe, and $TiSe_2$ crystals were employed as standards. Measurements of the temperature dependence of the electrical resistivity and specific heat were performed in a Quantum Design physical property measurement system (PPMS). Zero-field cooled (ZFC) and field cooled (FC) magnetic susceptibilities were measured in a field of 10 Oe using a Quantum Design superconducting quantum interference device (SQUID) magnetometer.

The electronic band spectra were obtained from ARPES measurements along highsymmetry direction Gamma-M at beamline 10 of the Advanced Light Source, Berkeley, using a Scienta R4000 analyzer at photon energies of 78 eV (1T crystals) and 47 eV (misfit compounds). Sample cleaving and data collection were performed in an ultrahigh vacuum of 5×10^{-9} Pa at $T = 15$ K.

3. Results and Discussion

Figure 1 shows the comparison of the Pb/Ti and Sn/Ti ratios obtained from the EDX measurements compared to the starting material compositions. The Pb/Ti and Sn/Ti ratios obtained from the EDX results were found to be within experimental error of the ratios present in the starting materials, indicating that the compositions of the $(Pb_{1-x}Sn_xSe)_{1.16}(TiSe_2)_2$ crystals and polycrystals grown between $x = 0$ and 0.6 for the synthetic method described are within error of the nominal compositions. Single phase crystals of the $(Pb_{1-x}Sn_xSe)_{1.16}(TiSe_2)_2$ misfit phase could only be obtained by our method up to $x = 0.6$. For higher x, the $((Pb,Sn)Se)_{1.16}(TiSe_2)_2$ misfit crystals were multiple-phase. Pure crystals of $(SnSe)_{1.16}(TiSe_2)_2$ were also obtained, but they were not superconducting above 1.8 K, and are not the subject of this study.

A representative room temperature X-ray diffraction pattern (PXRD), obtained from a crystal plate of $(Pb_{0.6}Sn_{0.4}Se)_{1.16}(TiSe_2)_2$ (example shown in the inset), looking at diffraction from the (00l) planes, is shown in Fig. 2. The pattern is very similar to that reported previously for the known $TiSe_2$ double layer misfit $(PbSe)_{1.16}(TiSe_2)_2$[24] and other misfit phases.[8] The structure of $(PbSe)_{1.16}(TiSe_2)_2$ has previously been described[24] and is not re-determined here.

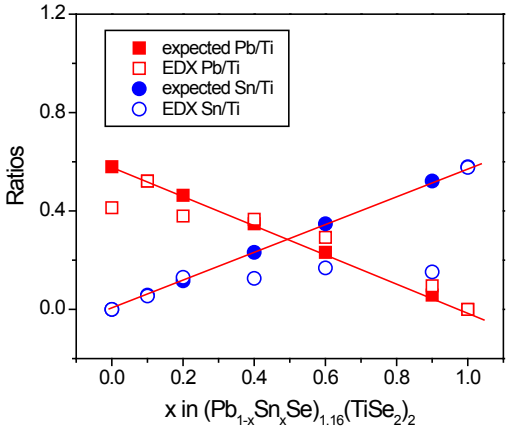

Fig. 1. (Color online) Comparison of the starting material Pb/Ti and Sn/Ti ratios with the EDX analysis of the single crystals grown of the misfit phase $(Pb_{1-x}Sn_xSe)_{1.16}(TiSe_2)_2$ $(0 \le x \le 0.6)$.

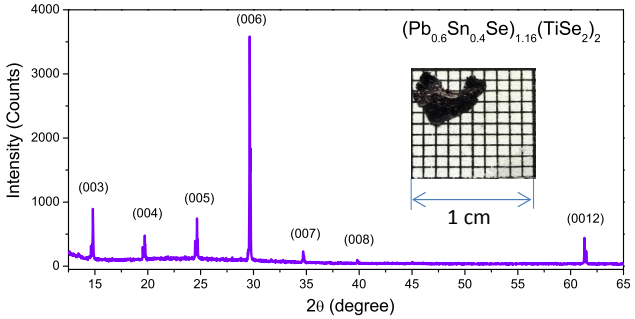

Fig. 2. (Color online) XRD pattern showing the (00L) reflections for a selected single crystal of $(Pb_{0.6}Sn_{0.4}Se)_{1.16}(TiSe_2)_2$. Inset, an example of a crystal plate of $(Pb_{0.6}Sn_{0.4}Se)_{1.16}(TiSe_2)_2$.

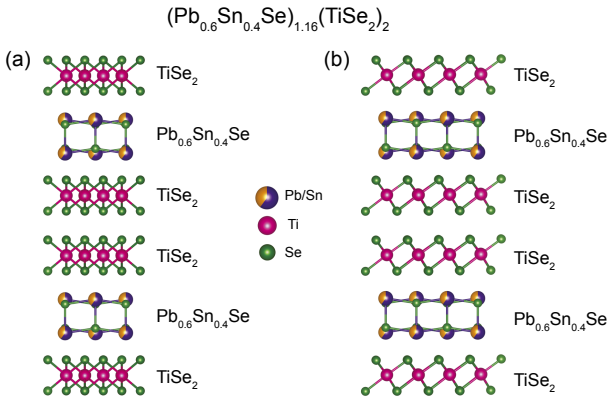

Fig. 3. (Color online) Schematic of the crystal structure of $(Pb_{1-x}Sn_xSe)_{1.16}(TiSe_2)_2$ $(x = 0.4)$, (a) along the b-direction; and (b) along the a-direction. The figures highlight the rocksalt double layers and the two 1T-like $TiSe_2$ layers whose interlayering generates the crystal structure of the misfit phase, while also showing that the in-plane matching of the layers in these directions is incommensurate.

Figures 3(a) and 3(b) show schematics of the misfit crystal structure of the $(Pb_{1-x}Sn_xSe)_{1.16}(TiSe_2)_2$, (using the example of $x = 0.4$) viewed in different directions. The figures highlight the basic structure as an alternating stacking of $(Pb_{1-x}Sn_x)Se$ rocksalt-type bi-layers with two 1T-like $TiSe_2$ layers, and also the incommensurate nature of their in-plane matching.

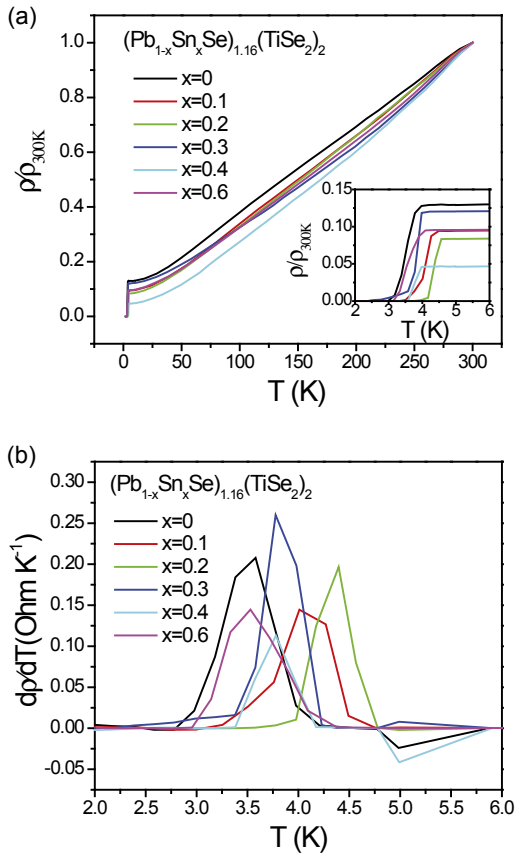

Fig. 4. (Color online) Transport characterization of the normal states and superconducting transitions. (a) The temperature dependence of the resistivity ratio (ρ/ρ_{300K}) for polycrystalline $(Pb_{1-x}Sn_xSe_2)_{1.16}(TiSe_2)_2$ ($0.0 \le x \le 0.6$), including the low temperature region (2–5.5 K); (b) $d\rho/dT$ for $(Pb_{1-x}Sn_xSe_2)_{1.16}(TiSe_2)_2$ ($0.0 \le x \le 0.6$) in the low temperature region (2–5.5 K), showing the information used to determine the superconducting transition temperatures.

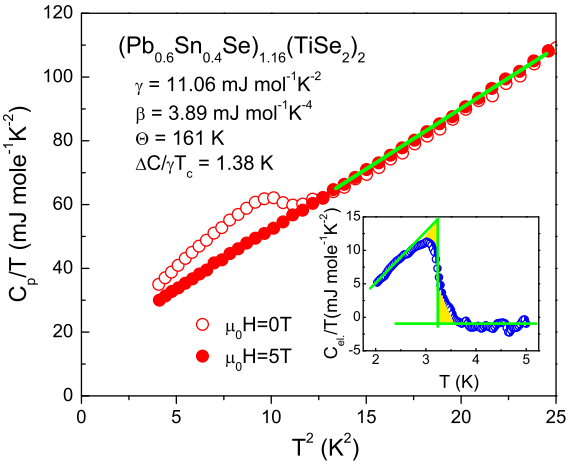

Fig. 5. (Color online) Low temperature specific heat characterization of $(Pb_{0.6}Sn_{0.4}Se)_{1.16}(TiSe_2)_2$. Temperature dependence of the specific heat C_p of a single crystal of $(Pb_{0.6}Sn_{0.4}Se)_{1.16}(TiSe_2)_2$ measured under magnetic fields of 0 and 5 T, presented in the form of C_p/T vs T^2. The values of γ and β (see text) were obtained by fitting the heat capacity data obtained in the range 2–5 K in the magnetic field of 5 T. The inset shows the electronic specific heat and the equal area construction employed to determine $\Delta C/\gamma T_c$.

Figure 4 shows the systematic change in the transport properties of $(Pb_{1-x}Sn_xSe)_{1.16}(TiSe_2)_2$ on increasing x. Figure 4(a) shows the temperature dependence of the resistivity ratio (ρ/ρ_{300K}) for polycrystalline $(Pb_{1-x}Sn_xSe_2)_{1.16}(TiSe_2)_2$ ($0.0 \le x \le 0.6$). The inset to the figure enlarges the resistivity behavior in the low temperature region (2–5.5 K); showing the superconducting transition. Figure 4(b) shows the $d\rho/dT$ for $(Pb_{1-x}Sn_xSe)_{1.16}(TiSe_2)_2$ ($0.0 \le x \le 0.6$) in the low temperature region (2–5.5 K), further showing the superconducting transition. At low temperatures, a clear, sharp ($\Delta T_c < 0.5$ K) drop of $\rho(T)$ is observed, signifying the onset of superconductivity. The T_c changes just slightly with the increase of doped Sn content x, displaying a very weak dome-shaped peak at intermediate compositions. We note that the T_c observed here for $x = 0$ is higher than the one previously reported for that material.[24] The reason for the improved T_c is not currently known but differences in the synthetic method may be behind the difference: there may be defects in the rocksalt layers that impact the amount of charge donated to the $TiSe_2$ layers.

The characterization of the superconducting properties of single crystal $(Pb_{0.6}Sn_{0.4}Se)_{1.16}(TiSe_2)_2$ by specific heat is shown in Fig. 5. Figure 5(a) shows the temperature dependence of the specific heat (C_p/T versus T^2) under zero-field and under a 5 T field for $(Pb_{0.6}Sn_{0.4}Se)_{1.16}(TiSe_2)_2$.

The normal state specific heat at low temperatures (but above T_c) obeys the relation of $C_p = \gamma T + \beta T^3$, where γ and β characterize the electronic and phonon contributions, respectively, the latter of which is a measure of the Debye temperature (θ_D). By fitting the data in the temperature range of 2–5 K, we obtain the electronic specific heat coefficient $\gamma = 11.06\,mJ{\cdot}mol^{-1}{\cdot}K^{-2}$ for $(Pb_{0.6}Sn_{0.4}Se)_{1.16}(TiSe_2)_2$. Per $TiSe_2$ layer, this number ($11.06/2 \sim 5.5\,mJ{\cdot}mol^{-1}{\cdot}K^{-2}$) is larger than that found for other superconductors based on $TiSe_2$ (i.e., $4.3\,mJ{\cdot}mol^{-1}{\cdot}K^{-2}$ for $Cu_{0.08}TiSe_2$[26] and $2\,mJ{\cdot}mol^{-1}{\cdot}K^{-2}$ for $Ti_{0.8}Ta_{0.2}Se_2$[27]).

The superconducting transition temperature observed in the specific heat measurements for $(Pb_{0.6}Sn_{0.4}Se)_{1.16}(TiSe_2)_2$ is in excellent agreement with the T_c determined in the $\rho(T)$ measurements. From the inset in Fig. 5, using the equal area construction method, we obtain $\Delta C/T_c = 11.28$ $mJ{\cdot}mol^{-1}{\cdot}K^{-2}$ for $(Pb_{0.6}Sn_{0.4}Se)_{1.16}(TiSe_2)_2$. The normalized specific heat jump value $\Delta C/\gamma T_c$ is thus found to be 1.38 for $(Pb_{0.6}Sn_{0.4}Se)_{1.16}(TiSe_2)_2$, which confirms the bulk superconductivity. This value is slightly smaller than that of the Bardeen–Cooper–Schrieffer (BCS) weak-coupling limit value (1.43), but is in a range typically observed in complex materials. Using the Debye temperature (θ_D), the critical temperature T_c, and assuming that the electron–phonon coupling constant (λ_{ep}) can be calculated from the inverted McMillan formula:[28]

$$\lambda_{ep} = \frac{1.04 + \mu^* \ln\left(\frac{\theta_D}{1.45T_c}\right)}{(1 - 0.62\mu^*)\ln\left(\frac{\theta_D}{1.45T_c}\right) - 1.04},$$

the value of λ_{ep} obtained is 0.72 for $(Pb_{0.6}Sn_{0.4}Se_2)_{1.16}(TiSe_2)_2$. This suggests weak coupling superconductivity. The density of states at the Fermi level [$N(E_F)$] can be calculated from the following equation:

$$N(E_F) = \frac{3}{\pi^2 k_B^2 (1 + \lambda_{ep})}\gamma,$$

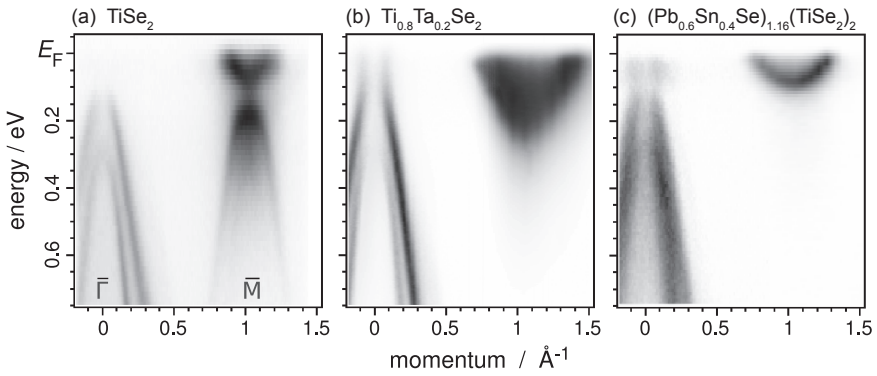

Fig. 6. Electronic band structures of (a) $TiSe_2$, (b) $Ti_{0.8}Ta_{0.2}Se_2$, and (c) $(Pb_{0.6}Sn_{0.4}Se)_{1.16}(TiSe_2)_2$ as determined by ARPES, at 15 K. All spectra are sampling the electronic states around $k_c = \pi/c$.

by using the value of Sommerfeld parameter (γ) and the electron–phonon coupling (λ_{ep}). This yields $N(E_F) = 2.73$ states/eV f.u. for $(Pb_{0.6}Sn_{0.4}Se_2)_{1.16}(TiSe_2)_2$.

ARPES data comparing the electronic structures of the host $TiSe_2$ material and two doped superconducting materials based on $TiSe_2$ is presented in Fig. 6. The $TiSe_2$ data is equivalent with those presented in previous reports[29,30] and shows the band folding that creates an echo of the valence band at Γ to the M point that is due to the CDW in the host material. The $Ti_{0.8}Ta_{0.2}Se_2$ data show the same basic electronic structure, but now with the CDW strongly suppressed (the echo of the valence band at Γ is much weaker at the M point), and a significant degree of filling of the conduction band at the M points. The electronic band structure of $(Pb_{0.6}Sn_{0.4}Se)_{1.16}(TiSe_2)_2$ [Fig. 6(c)] shows all the features characteristic of bulk $TiSe_2$ and $Ti_{0.8}Ta_{0.2}Se_2$ [Figs. 6(a) and 6(b)]: two (three at other k_c are not shown here) hole-like bands in the center of the Brillouin zone and electron pockets centered at six M points of the Brillouin zone are seen. No bands that can be ascribed to the $(Pb_{1-x}Sn_x)Se$ layers are observed at the measured Fermi surface of the misfit phase: no fourfold symmetry in the low-energy band structure is present. The cleavage of $(Pb_{0.6}Sn_{0.4}Se)_{1.16}(TiSe_2)_2$ most likely results in single-layer $TiSe_2$ termination of the cleaved crystal because the double $TiSe_2$ layers are separated by a weakly bonded van der Waals gap. Thus The complete absence of (Pb,Sn)Se states is probably due to short probing depth at the photon energies employed the (PbSn)Se layers are too deep to be probed and are not exposed in the cleave. Comparing the electron pocket in the misfit phase with that of Ta-doped $TiSe_2$ [Figs. 6(b) and 6(c)] shows that the conduction band is occupied to a lesser degree in the misfit. The CDW-generated replica of the hole pocket is well developed at the M-point of the Brillouin zone in $TiSe_2$ and is only weakly present, in both the Ta doped and misfit phases, where it exists to near room temperature in the latter. The implication of the ARPES data is that the CDW amplitude in the $TiSe_2$ layers is substantially suppressed, although not completely disrupted, in both doped superconducting phases.

Finally, the electronic phase diagram as a function of temperature and doping level for the $(Pb_{1-x}Sn_xSe)_{1.16}(TiSe_2)_2$ misfit phase series is summarized in Fig. 7. It can be seen that in the $(Pb_{1-x}Sn_xSe)_{1.16}(TiSe_2)_2$ system, the x dependence of T_c displays a dome-like shape that is broad in composition.

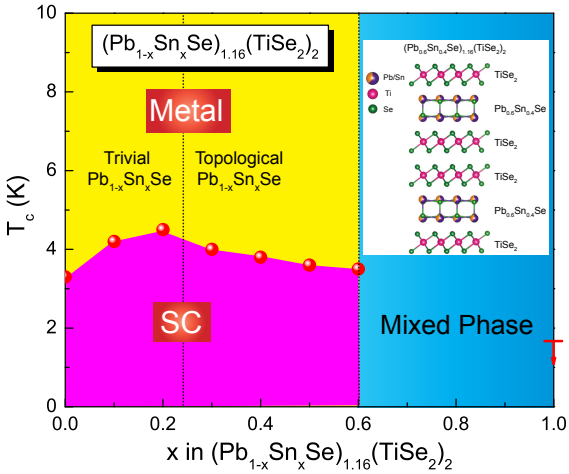

Fig. 7. (Color online) The T_c vs Sn content x of the superconductor in the $(Pb_{1-x}Sn_xSe)_{1.16}(TiSe_2)_2$ misfit system. The composition of the trivial to topological transition in bulk rocksalt $Pb_{1-x}Sn_xSe$ is shown by a dashed line.

However, T_c changes only slightly with the increase content of doped Sn x, with a maximum T_c of 4.5 K at $x = 0.2$. If there is any change on crossing the trivial to topological composition regime in bulk $Pb_{1-x}Sn_xSe$ at $x = 0.25$ it is only a subtle change in the slope of T_c vs x near the top of the dome. For $x = 0.4$, well into the topological regime of bulk $Pb_{1-x}Sn_xSe$, the misfit material remains superconducting. Whether the band structure of (Pb,Sn)Se layers in the misfit is of the trivial or topological type remains to be seen in future study. For compositions between $x = 0.6$ and 1.0 we could not obtain single phase materials by our synthetic method, and thus no data is shown in Fig. 7 for higher x; single phase misfit material was obtained at $x = 1$ [i.e., $(SnSe)_{1.16}$-$(TiSe_2)_2$], but we did not observe any superconducting transition down to 2 K.

4. Conclusion

The misfit phase $(Pb_{1-x}Sn_xSe)_{1.16}(TiSe_2)_2$ $(0 \le x \le 0.6)$ series, which combines layers of the rocksalt structure topological crystalline insulator $Pb_{1-x}Sn_xSe$ with the layers of the transition metal dichalcogenide $TiSe_2$, is reported, and the trends in superconductivity in the series characterized. The superconducting transition temperature shows a weak dome shape with varying x, with a maximum $T_c \approx 4.5$ K close to the composition of the trivial to inverted transition in

the band structure of bulk rocksalt $Pb_{1-x}Sn_xSe$. For the misfit superconductor $(Pb_{0.6}Sn_{0.4}Se)_{1.16}(TiSe_2)_2$, whose Pb:Sn ratio is well within the topological composition regime of the bulk rocksalt material, the Sommerfeld parameter $\gamma = 11.06$ $mJ{\cdot}mol^{-1}{\cdot}K^{-2}$, the Debye temperature $\Theta_D = 161$ K, the normalized specific heat jump value $\Delta C/\gamma T_c = 1.38$ and the electron–phonon constant value $\lambda_{ep} = 0.72$, suggesting that $(Pb_{0.6}Sn_{0.4}Se)_{1.16}(TiSe_2)_2$ is a BCS-type weak coupling superconductor. No superconducting transition is observed for the $(SnSe)_{1.16}(TiSe_2)_2$ misfit above 1.8 K. Why the SnSe-based misfit material is not superconducting at temperatures comparable to those exhibited by the Pb+Sn containing misfit phases is not currently known. Further work that investigates the electronic state of the $Pb_{1-x}Sn_xSe$ layers in the misfit phase, to see whether they indeed host topological states, would be of interest. If they do, then interaction of those topological states with the superconductivity would be of future interest.

Acknowledgements

The materials synthesis and physical property characterization of this superconductor were supported by the Department of Energy, division of basic energy sciences, Grant DE-FG02-98ER45706. The ARPES work was supported by the ARO MURI on topological insulators grant W911NF-12-0461. The authors acknowledge discussions with Ali Yazdani.

*huixial@princeton.edu
†rcava@princeton.edu

1) R. L. Withers and L. A. Bursil, Philos. Mag. B **43**, 635 (1981).
2) G. A. Wiegers and W. Y. Zhou, Mater. Res. Bull. **26**, 879 (1991).
3) W. Y. Zhou, A. Meetsma, J. L. de Boer, and G. A. Wiegers, Mater. Res. Bull. **27**, 563 (1992).
4) R. Atkins, S. Disch, Z. Jones, I. Haeusler, C. Grosse, S. F. Fischer, W. Neumann, P. Zschack, and D. C. Johnson, J. Solid State Chem. **202**, 128 (2013).
5) F. R. Harris, S. Standridge, and D. C. Johnson, J. Am. Chem. Soc. **127**, 7843 (2005).
6) N. S. Gunning, J. Feser, M. Falmbigl, M. Beekman, D. G. Cahill, and D. C. Johnson, Semicond. Sci. Technol. **29**, 124007 (2014).
7) T. Kondo, K. Suzuki, and T. Enoki, Solid State Commun. **84**, 999 (1992).
8) G. A. Wiegers, A. Meesma, R. J. Haange, S. V. Smaalen, and J. L. De Boer, Acta Crystallogr., Sect. B **46**, 324 (1990).
9) Y. Gotoh, M. Goto, K. Kawaguchi, Y. Oosawa, and M. Onoda, Mater. Res. Bull. **25**, 307 (1990).
10) M. Onoda, K. Kato, Y. Gotoh, and Y. Oosawa, Acta Crystallogr., Sect. B **46**, 487 (1990).
11) Y. Gotoh, J. Akimoto, M. Sakurai, Y. Kiyozumi, K. Suzuki, and Y. Oosawa, Chem. Lett. **19**, 2057 (1990).
12) Y. Gotoh, J. Akimoto, Y. Oosawa, and M. Onoda, Jpn. J. Appl. Phys. **34**, L1662 (1995).
13) N. T. Nguyen, B. Howe, J. R. Hash, N. Liebrecht, P. Zschack, and D. C. Johnson, Chem. Mater. **19**, 1923 (2007).
14) Y. Oosawa, Y. Gotoh, J. Akimoto, M. Sohma, T. Tsunoda, H. Hayakawa, and M. Onoda, Solid State Ionics **67**, 287 (1994).
15) D. B. Moore, M. Beekman, S. Disch, and D. C. Johnson, Angew. Chem., Int. Ed. **53**, 5672 (2014).
16) K. Takita and K. Masuda, J. Low Temp. Phys. **58**, 127 (1985).
17) P. Dziawa, B. J. Kowalski, K. Dybko, R. Buczko, A. Szczerbakow, M. Szot, E. Łusakowska, T. Balasubramanian, B. M. Wojek, M. H. Berntsen, O. Tjernberg, and T. Story, Nat. Mater. **11**, 1023 (2012).
18) W. W. Yu, J. C. Falkner, B. S. Shih, and V. L. Colvin, Chem. Mater. **16**, 3318 (2004).
19) Y. Oosawa, Y. Gotoh, J. Akimoto, T. Tsunoda, M. Sohma, and M. Onoda, Jpn. J. Appl. Phys. **31**, L1096 (1992).
20) F. J. Di Salvo, D. E. Moncton, and J. V. Waszczak, Phys. Rev. B **14**, 4321 (1976).
21) N. G. Stoffel, S. D. Kevan, and N. V. Smith, Phys. Rev. B **31**, 8049 (1985).
22) J. A. Wilson, Solid State Commun. **22**, 551 (1977).
23) T. E. Kidd, T. Miller, M. Y. Chou, and T. C. Chiang, Phys. Rev. Lett. **88**, 226402 (2002).
24) N. Giang, Q. Xu, Y. S. Hor, A. J. Williams, S. E. Dutton, H. W. Zandbergen, and R. J. Cava, Phys. Rev. B **82**, 024503 (2010).
25) J. Rodríguez-Carvajal, Commun. Powder Diffr. **26**, 12 (2001).
26) E. Morosan, H. W. Zandbergen, B. S. Dennis, J. W. G. Bos, Y. Onose, T. Klimczuk, A. P. Ramirez, N. P. Ong, and R. J. Cava, Nat. Phys. **2**, 544 (2006).
27) H. X. Luo, W. W. Xie, J. Tao, I. Pletikosic, T. Valla, G. S. Sahasrabudhe, G. Osterhoudt, E. Sutton, K. S. Burch, E. M. Seibel, J. W. Krizan, Y. M. Zhu, and R. J. Cava, Chem. Mater. **28**, 1927 (2016).
28) W. L. McMillan, Phys. Rev. **167**, 331 (1968).
29) S. Negishi, H. Negishi, K. Shimada, X. Y. Cui, M. Higashiguchi, M. Nakatake, M. Arita, H. Namatame, M. Taniguchi, A. Ohnishi, and M. Sasaki, Physica B **383**, 155 (2006).
30) J. van Wezel, P. Nahai-Williamson, and S. S. Saxena, EPL **89**, 47004 (2010).